Analyzing Topography of Membrane-Inserted Diphtheria Toxin T Domain Using BODIPY-Streptavidin: At Low pH, Helices 8 and 9 Form a Transmembrane Hairpin but Helices 5−7 Form Stable Nonclassical Inserted Segments on the cis Side of the Bilayer†

Michael P. Rosconi, Gang Zhao, and Erwin London*

Department of Biochemistry and Cell Biology and Department of Chemistry, State University of New York at Stony Brook, Stony Brook, New York 11794-5215

Received April 2, 2004; Revised Manuscript Received May 7, 2004

ABSTRACT: Low pH-induced membrane insertion by diphtheria toxin T domain is crucial for A chain translocation into the cytoplasm. To define the membrane topography of the T domain, the exposure of biotinylated Cys residues to the cis and trans bilayer surfaces was examined using model membrane vesicles containing a deeply inserted T domain. To do this, the reactivity of biotin with external and vesicle-entrapped BODIPY-labeled streptavidin was measured. The T domain was found to insert with roughly 70−80% of the molecules in the physiologically relevant orientation. In this orientation, residue 349, located in the loop between hydrophobic helices 8 and 9, was exposed to the trans side of the bilayer, while other solution-exposed residues along the hydrophobic helices 5−9 region of the T domain located near the cis surface. A protocol developed to detect the movement of residues back and forth across the membranes demonstrated that T domain sequences did not rapidly equilibrate between the cis and the trans sides of the bilayer. Binding streptavidin to biotinylated residues prior to membrane insertion only inhibited T domain pore formation for residues in the loop between helices 8 and 9. Pore formation experiments used an approach avoiding interference from transient membrane defects/leakage that may occur upon the initial insertion of protein. Combined, these results indicate that at low pH hydrophobic helices 8 and 9 form a transmembrane hairpin, while hydrophobic helices 5−7 form a nonclassical deeply inserted nontransmembraneous state. We propose that this represents a novel pre-translocation state that is distinct from a previously defined post-translocation state.

Diphtheria toxin (DT) is a protein toxin secreted by the bacterium *Corynebacterium diphtheriae*. The mature toxin (58 kDa) consists of two polypeptide chains, A (21 kDa) and B (37 kDa), which are joined by a single disulfide bond. The toxin consists of three distinct domains: the A chain is identical to the catalytic (C) domain of the protein while the B chain consists of two domains, the receptor binding domain (R) and the transmembrane (T) domain (*1*−*4*). Upon entering endosomes via receptor-mediated endocytosis, a conformational change triggered by the low pH of the endosomal lumen renders the toxin hydrophobic. This results in membrane penetration by the toxin and subsequent translocation of the A chain into the cytosol. The cytosolic A chain catalyzes the ADP ribosylation of the diphthamide residue of elongation factor 2, which shuts down protein synthesis and leads to cell death (*5*). The translocation process can also be observed in a cell free system suggesting that the toxin alone possesses the ability to penetrate and transverse lipid bilayers (*6*−*9*), although it may be aided to some degree (*10*). The study of this system may allow us to better elucidate the poorly understood process of protein translocation across biological membranes.

Much of the recent research on the toxin has focused on the largely α-helical T domain. The T domain is believed to have a critical role in the translocation of the A chain. It has a distinctively hydrophobic C-terminal portion and has the ability to spontaneously insert into, and form pores within, both biological and model membranes at low pH (*11*−*14*). Thus, studying the topography of the T domain in the membrane-inserted state is of particular interest. Determination of which segments span the membrane is likely to provide insights into their role in translocation. It was originally predicted that there would be two transmembrane hairpins formed from four long hydrophobic sequences in the C-terminal portion of the T domain (*1*). One hairpin would be formed by the hydrophobic helices 8 and 9 (TH8 and TH9). The second would consist of TH5 and a combination of two shorter helices, TH6 and TH7 (Figure 1). Although a wide variety of techniques suggest that TH8 and TH9 form a transmembrane helical hairpin (*15*−*24*), the behavior of TH5−7 remains unclear. We previously found that the natural Trp in the center of TH5 inserted into lipid bilayers (*25*). Evidence for TH5 insertion was also derived from hydrophobic photolabeling studies (*26*). Senzel et al. have recently suggested that TH5 spans the membrane, along with TH8,9, when the T domain forms open channels in planar lipid bilayers (*27*). However, because the T domain

† This work was supported by NIH Grant GM 31986.

* To whom correspondence should be addressed. Tel: 631-632-8564. Fax: 631-632-8575. E-mail: Erwin.London@stonybrook.edu.

10.1021/bi049354j CCC: $27.50
Published on Web 06/22/2004

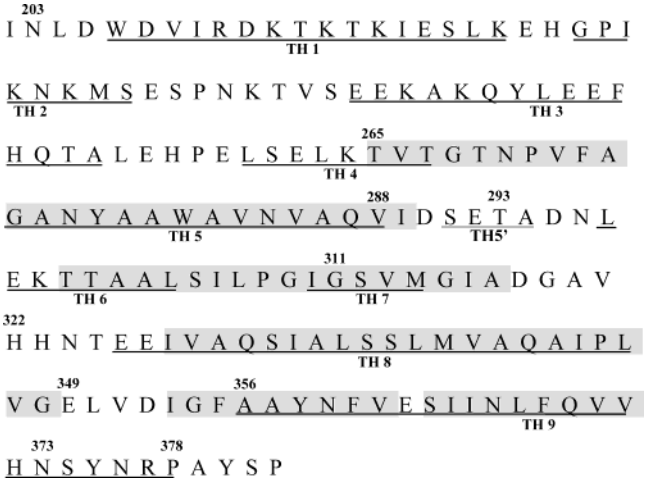

FIGURE 1: Sequence of the DT T domain. Sequences forming helices TH1−9 according to the DT crystal structure (*2*) are shown underlined. The numbers above the residues are sites of some of the single Cys mutations studied in this report. The uncharged segments are shown shaded.

can adopt several different conformations (see below), the topography that they observe may correspond to a state that exists at only one of several steps in translocation (see Discussion).

We have established that the membrane-inserted T domain can exist in two distinct conformations. In the P state, hydrophobic helices 5−9 lay close to the membrane surface, while in the TM state they insert more deeply (*28*−*30*). Bilayer width, bilayer curvature, T domain concentration, and interaction with molten globule-like proteins affect which state predominates (*28*, *29*, *31*). While our previous data on the topography of TH8 and TH9 in the more deeply inserting state were consistent with a transmembrane hairpin, our data on TH5−7 in the same state were consistent with two deeply inserted but nontransmembraneous segments. One deeply inserted segment corresponded to TH5, and the other correspondend to the TH6/7 sequence. However, a critical ambiguity could not be resolved in these experiments. This ambiguity involved the possibility that a dynamic equilibrium between transmembraneous and nontransmembraneous conformations of TH5 and/or TH6/7 exists.

This ambiguity is symptomatic of the fact that protein toxins are, in general, the most challenging targets for topography experiments in membranes due to their topographical flexibility (see Discussion). Thus, new and more sophisticated methods are needed for achieving comprehensive topographical analysis of toxins, a very important class of membrane proteins. The binding of streptavidin (SA) to biotinylated residues has proved to be a powerful approach to understanding DT topography (*8*, *27*, *32*). In this study, we modified an elegant spectroscopic BODIPY (BOD)-avidin approach (*33*−*35*) to identify biotinylated T domain residues that reach the trans side of the bilayer upon membrane insertion. Importantly, a modification of the assay was developed to allow the determination of whether portions of the T domain can equilibrate back and forth across the bilayer (*30*). The results indicated that TH8 and TH9 adopt a stable transmembrane structure at low pH whereas TH5−7 form a stable deeply inserted structure that is nontransmembraneous. Studies of the effect of binding SA to the biotinylated T domain residues prior to membrane insertion upon pore formation by the T domain were consistent with this model.

EXPERIMENTAL PROCEDURES

Materials. Dioleoylphosphatidylcholine (DOPC), dimyristoleoylphosphatidylcholine (DMoPC), dioleoylphosphatidylglycerol (DOPG), and N-lissamine rhodamine-dipalmitoylphosphatidylethanolamine (rhodamine-PE) were purchased from Avanti Polar Lipids (Alabaster, AL). The lipid concentrations were determined by dry weight. SA BOD fluorescence conjugate (BOD-SA) (discontinued except as a custom labeling product), SA, *N*-(biotinoyl)-*N*′-(iodoacetyl)-ethylenediamine (biotin-IA), rabbit anti-Cascade Blue (CB) IgG, 8-methoxypyrene-1,3,6-trisulfonic acid, trisodium salt (MPTS or CB dye), and Texas Red-X succinimidyl ester (TxR-SE) were purchased from Molecular Probes (Eugene, OR). *N*-(6-(Biotinamido)hexyl)-3′-(2′-pyridyldithio)propionamide (EZ-Link Biotin-HPDP, biotin-HPDP) was obtained from Pierce Biotechnology (Rockford, IL). All other chemicals were reagent grade.

Site-Directed Mutagenesis and Protein Purification. Plasmids coding for T domains with single Cys substitutions were constructed, and the T domain protein was expressed and purified as previously described (*30*). *Escherichia coli* BL21 cells transformed with each respective mutant were stored in 15% glycerol at −80 °C. The plasmids coding for T domain mutants 322, 349, 356, 373, and 378 were a gift from the lab of Dr. R. J. Collier (Harvard Medical School). Purified protein was stored as a stock solution in the FPLC elution buffer (10 mM Tris-Cl and about 150−250 mM NaCl, pH 8.2) at −20 °C and at a protein concentration of 1.5−2.5 mg/mL.

Biotinylation of T Domain Mutants. The T domain mutants were labeled with the cysteine specific biotinylation probes. Typically, 40−80 μL of 8 mM biotin-IA or biotin-HPDP dissolved in dimethyl sulfoxide was added to enough of the T domain mutant stock solution to give a total volume of 1 mL (6:1 mole ratio label:protein). After a 1h incubation at room temperature the sample was then dialyzed, using dialysis tubing (Spectra/Por) with a molecular weight cutoff of 8000, against 4 L of Tris buffer (10 mM Tris-Cl, 150 mM NaCl, pH 8.2), with no change of buffer, to remove the excess unbound probe. All dialysis steps were performed at 4 °C. Affinity chromatography was then performed using a monomeric avidin column (Pierce Biotechnology) to remove any unbiotinylated T domain protein. The column was packed according to the procedure provided by the manufacturer except that a column volume of 0.5 mL was used. The sample was passed over the column, and the flow through was collected and passed over the column again. This was repeated six times to improve the binding efficiency. The biotinylated protein was eluted from the column with six separate 0.6 mL aliquots of 0.1 M phosphate, 0.15 M NaCl, and 5 mM biotin, pH 7 (biotin elution buffer). The eluate fractions were collected for each aliquot added and subjected to sodium dodecyl sulfate polyacrylamide gel electrophoresis (SDS−PAGE). Those fractions containing the most biotinylated protein were pooled. The pooled fractions were dialyzed against 5 L of Tris buffer, pH 8.2, over a 24 h period with two buffer changes to remove the free biotin. Extensive dialysis was critical to remove the

contaminating biotin. The protein concentration was then determined using the Bradford colorimetric assay (Bio-Rad, Hercules, CA). The final concentrations ranged from 0.1 to 0.5 mg/mL protein.

Titration of BOD-SA with Free Biotin and Biotinylated T Domain. The dependence of the interaction of biotin with BOD-SA upon biotin concentration was monitored by the increase in BOD fluorescence upon biotin binding. BOD-SA (1 mg/mL in Tris buffer, pH 8.2) was diluted to 700 μL with either Tris buffer (10 mM Tris-Cl, 150 mM NaCl, pH 8.0) or acetate buffer (6.7 mM Tris-Cl, 167 mM acetate, and 150 mM NaCl, pH 4.5) to give a final BOD-SA concentration of 0.15 μg/mL.

In some samples, small unilamellar vesicles (SUV), prepared by sonication as described previously (*29*), were also present. The samples containing SUV were prepared by diluting BOD-SA to 700 μL as described above with a mixture of buffer and an aliquot of a stock solution of 70% DOPC, 30% DOPG (mol:mol), and SUV (10 mM total lipid) dispersed in the same buffer to give a final lipid concentration of 200 μM. To these BOD-SA-containing solutions, sequential small aliquots ($\leq$2 μL) of a solution of either free biotin/water or 0.5 mg/mL biotin-labeled T domain 378 ($T_{378-biotin-IA}$) dissolved in Tris buffer, pH 8.2, were then added and mixed. At these small volumes, Tris buffer effects on sample pH were negligible. The BOD fluorescence was measured after the addition of each aliquot once its fluorescence stabilized (5−30 min).

Kinetics of BOD-SA Reaction with Free Biotin and Biotinylated T Domain. A small aliquot from a stock solution of 7 μM free biotin/water or 0.5 mg/mL $T_{378-biotin-IA}$ dissolved in Tris buffer, pH 8.2, was added to 700 μL of acetate buffer, pH 4.5, containing 0.15 μg/mL BOD-SA and SUV composed of 200 μM 7:3 DOPC:DOPG (mol/mol). The aliquot added (0.02 μM biotin) gave a ratio of two biotins per biotin binding site on BOD-SA. The BOD fluorescence intensity was measured every 10 s until the intensity stabilized.

Assaying SA Binding to Biotinylated T Domain Mutants. Because SA and the T domain form a complex that is stable on SDS gels (*8*), SA binding to biotinylated T domain mutants was assayed by the disappearance of the free T domain band on an SDS polyacrylamide gel upon the addition of SA. A 10 μL sample containing 0.1 mg/mL biotinylated T domain was prepared by dilution (if necessary) of a stock solution of biotinylated T domain with additional Tris buffer, pH 8.2, or by dilution with a mixture of Tris buffer and a 3 μL aliquot from a 2 mg/mL solution of SA/water. After the mixture was incubated for 15 min at room temperature, 0.5 μL of 10 mM D-biotin was added to the SA-containing samples to inactivate excess SA. After the appropriate aliquot of 4X loading buffer (*8*) was added, SDS−PAGE was performed using precast 8−25% Phastgels on a Phastsystem instrument (Pharmacia Biotech) and visualized using Coomasie Blue staining.

Entrapping BOD-SA or Anti-CB Antibodies in Model Membrane Vesicles. BOD-SA was trapped inside large unilamellar vesicles (LUV) formed by octylglucoside (OG) dialysis (*8*, *11*) at 4 °C. The LUV were composed of 70%DOPC/30%DOPG (mol/mol) and 0.02% rhodamine-PE, the latter being used as a fluorescent marker of lipid. To 10 μmol of dried lipid were added 20 mg of solid OG and either a 100 μL aliquot from a 1 mg/mL solution of BOD-SA dissolved in Tris buffer, pH 8.2, or a 14 μL aliquot from a 7 mg/mL solution of unlabeled SA dissolved in Tris buffer, pH 8.2. For the samples containing BOD-SA, a subsaturating 4.5 μL aliquot from a solution containing 210 μM D-biotin dissolved in 100 mM Na phosphate and 150 mM NaCl, pH 7.2, was added [0.5:1, biotin:BOD-SA (mol:mol)] to give a more linear response of BOD fluorescence enhancement upon binding to biotin (see Results for details). The samples were brought to a volume of 1 mL with acetate buffer, pH 4.5.

The samples were then dialyzed against 5 L of 50 mM Na acetate and 150 mM NaCl, pH 4.5 (dialysis buffer), and passed over a Sepharose 4B-CL column (0.5 cm radius, 40 cm length) to separate the free BOD-SA from the vesicle-entrapped BOD-SA. The samples were eluted from the column using the dialysis buffer, and the one or two fractions containing the most lipid were pooled. The free BOD-SA was saved for use in later experiments. The trapping efficiency was found to be about 10%, determined by BOD fluorescence. The final concentration of lipid and trapped BOD-SA was 3−5 mM and 2.8−4.7 μg/mL, respectively. BOD-SA remained trapped inside the vesicles for 3−4 weeks as assessed by a negligible BOD fluorescence increase (>5%) upon addition of externally added biotinylated 3 kDa dextran. [When an equivalent amount of BOD-SA was just dissolved in solution, the fluorescence increased severalfold when added to biotinylated dextran (not shown).] Unlabeled SA was trapped using the same procedure as for BOD-SA.

Anti-CB antibodies were trapped inside LUV using a protocol similar to that above. Immediately prior to dialysis, the concentration of anti-CB antibody was 3 mg/mL, the lipid concentration was 10 mM, and the OG concentration was 20 mg/mL, and all were dissolved in a final volume of 0.5 mL of phosphate-buffered saline, 10 mM Na_2HPO_4, 1.8 mM KH_2PO_4, 2.7 mM KCl, 137 mM NaCl pH 7.2, 5 mM azide. The dialysis/Sepharose 4B elution buffer was Tris buffer, pH 8.2. The trapping efficiency for anti-CB antibodies was about 10% as determined by antibody Trp fluorescence. The final concentrations of lipid and trapped anti-CB were 1−3 mM and 33−50 μg/mL (about 0.22−0.33 μM), respectively. Anti-CB antibodies remained trapped inside the LUV for 3−4 weeks as determined by the relative lack of quenching of CB fluorescence ($\leq$10%) upon addition of free CB to trapped anti-CB in the absence of the T domain.

Fluorescence Measurements. The fluorescence was measured at room temperature with a Spex 212 Fluorolog spectrophotometer operating in ratio mode. Unless otherwise noted, measurements were made in a semi-microquartz cuvette (excitation path length 10 mm, emission path length 4 mm). The excitation and emission slit widths used were 2.5 and 5 mm, respectively. The excitation and emission wavelength sets for Trp, BOD, CB, and Texas Red were [280, 335], [488, 516], [385, 417], and [580, 608] nm, respectively. The Trp fluorescence intensity was averaged over a 6 s period. For the other fluorophores, a 10−15 s period was used.

Interaction of Biotinylated T Domain Mutants with Externally Added and Vesicle-Entrapped BOD-SA. The degree of interaction of externally added BOD-SA with LUV-inserted biotinylated T domain mutants was determined as follows: a binding stock solution containing 20 μg/mL T

domain [composed of 18 μg/mL unlabeled "wild-type" T (WT T), which contains an N-terminal hexaHis tag but no Cys residues, plus 2 μg/mL biotinylated T domain] and LUV at a lipid concentration of 1.9−2.2 mM was prepared in a final volume of 80 μL. To do this, typically, 1.6−5.2 μL of a solution containing the T domain mixture in Tris buffer, pH 8.2, was added to LUV that were prepared in and diluted to 78.4−74.8 μL with acetate buffer, pH 4.5. The pH remained within 0.1 pH units of 4.5. The vesicles used had either no trapped protein (empty LUV) or trapped unlabeled SA (LUV/SA). Because the SA and BOD-SA trapping efficiencies were about equal (data not shown), the concentration of trapped unlabeled SA was about 2 μg/mL at this stage. The samples containing empty LUV were preincubated at this stage for 10 min while the LUV/SA samples were preincubated for 30 min.

In a separate tube, a 5−10 μL aliquot containing 0.14 μg of untrapped BOD-SA dissolved in dialysis buffer, pH 4.5, was made up to 630 μL with acetate buffer, pH 4.5. (The BOD-SA concentration was calculated by the BOD fluorescence intensity relative to that of a known dilution of the BOD-SA stock solution.) The BOD fluorescence of this sample was measured as described above. Then, the reaction between biotinylated T domain and BOD-SA was initiated by adding 70 μL of the above-described binding stock solution containing the vesicle-inserted T domain to the 630 μL of BOD-SA diluted with acetate buffer, while stirring, and the BOD fluorescence was remeasured at time intervals of 5, 10, and 30 min. The final concentrations were as follows: 0.19−0.22 mM lipid, 0.2 μg/mL biotinylated T domain, 1.8 μg/mL unlabeled WT T domain, 0.2 μg/mL external BOD-SA, and (when present) 0.2 μg/mL trapped unlabeled SA.

To assay the amount of interaction of biotinylated T domain mutants with LUV-entrapped BOD-SA (LUV/BOD-SA), a 40−60 μL aliquot of LUV/BOD-SA in dialysis buffer, pH 4.5, was diluted to 695−698 μL with acetate buffer, pH 4.5, and the initial fluorescence was measured. The exact volume of the BOD-SA aliquot was chosen to give a final concentration of 0.2 μg/mL as judged by its BOD fluorescence. Then, the reaction between biotinylated T domain and vesicle-entrapped BOD-SA was initiated by adding a 1.4−4.6 μL aliquot containing a mixture of 0.29 μg of biotinylated T domain and 2.6 μg of unlabeled WT T domain (both dissolved in Tris buffer, pH 8.2), while stirring. The fluorescence of the sample was recorded at time intervals of 5, 10, and 30 min. The final sample volume was 700 μL, and the concentrations of all components were the same as in the above-described samples containing external BOD-SA. The final pH remained within 0.1 pH units of 4.5. In experiments in which the behavior of biotin labels or free biotin were examined, the procedure was identical except that an equivalent concentration of biotin was used in place of the T domain.

We defined the % external reactivity from the following formula:

$$\%\ \text{external reactivity} = \{(F - F_o)_{ex}/[(F - F_o)_{ex} + (F - F_o)_{tr}]\} \times 100\%$$

where F is the BOD-SA fluorescence after reaction with biotin; F_o is the initial BOD-SA fluorescence (prior to the addition of biotin); $(F - F_o)_{ex}$ is the amount of BOD fluorescence increase observed in samples where BOD-SA was externally added to vesicles containing the biotinylated T domain; and $(F - F_o)_{tr}$ is the amount of BOD fluorescence increase observed in samples where the biotinylated T domain was added to vesicles with entrapped BOD-SA. Background intensities from samples lacking BOD-SA were subtracted to obtain the BOD fluorescence intensities, and for external BOD-SA experiments, BOD fluorescence values were corrected for the initial dilution by the vesicle-containing aliquot. Each experiment used duplicate samples and was performed two or three times for each condition tested.

Pore Formation Determined by CB Influx. The pore-forming ability of biotinylated T domain mutants was determined by CB influx into LUV containing trapped anti-CB antibodies. A 40−60 μL aliquot of LUV containing buffer or LUV containing entrapped anti-CB (prepared as described above) was diluted with acetate buffer, pH 4.5, to 300 μL less the volume of the T domain and CB to be added (see below). To this, a small aliquot (6−24 μL) of Tris buffer, pH 8.2, containing 1.2 μg of either biotinylated T domain or 1.2 μg of biotinylated T domain preincubated for 20 min. with 7 μg of SA was added while vortexing. After a 20 min. incubation, the sample was transferred to a microcuvette (excitation path length 4 mm, emission path length 4 mm), and the fluorescence intensity at CB wavelengths was measured to determine the background values. After the mixture was retransferred to a test tube, a 5−7 μL aliquot from a solution of 0.1 μM CB/Tris buffer, pH 8.2, was added. The final sample had a volume of 300 μL and contained 200 μM lipid, ~0.05 μM trapped anti-CB, ~2 nM CB, and 4 μg/mL T domain. The final pH remained 4.5. The sample was vortexed briefly and incubated for 1 h at room temperature before the fluorescence was remeasured. Finally, to determine the maximum amount of quenching possible, the fluorescence was remeasured after 6 μL of 200 mg/mL OG was added to disrupt the vesicles. The addition of OG did not affect the binding of CB to anti-CB (data not shown). The % of maximum quenching was calculated with the following formula:

$$\%\ \text{of maximum quenching} = \text{fraction quenching/fraction quenching in detergent} = \{[1 - (F_{anti-CB}/F_o)]/[1 - (F_{anti-CB-OG}/F_{o-OG})]\} \times 100\%$$

where F_o is the fluorescence of a sample containing empty LUV; $F_{anti-CB}$ is the fluorescence of a sample containing vesicle-entrapped anti-CB; $F_{anti-CB-OG}$ is the fluorescence of a sample containing vesicle-entrapped anti-CB after the addition of OG; and F_{o-OG} is the fluorescence in the samples containing empty LUV after the addition of OG. For each sample, three separate fluorescence readings were taken, with mixing between each reading, and averaged. Each experiment consisted of duplicate samples for each condition tested, and the experiments were performed 2−3 times.

Lipid Binding of Biotinylated T Domain Mutant 349 Assayed by Migration in a Sucrose Gradient. The binding of T domain biotinylated on residue 349 ($T_{349-biotin-IA}$) to LUV, with and without SA prebound to the T domain, was determined by migration in a sucrose gradient. To detect the T domain, $T_{349-biotin-IA}$ was labeled with TxR-SE. To do this,

a 0.5 mL aliquot of a 100 μg/mL solution of $T_{349-biotin-IA}$ was dialyzed against 5 L of 100 mM sodium carbonate and 150 mM NaCl, pH 8.3, buffer overnight to prevent TxR-SE reaction with the Tris in which the T domain was stored. Next, 6.3 μL of an 8 mM solution of TxR-SE dissolved in dimethyl sulfoxide was added to the biotin-349 T [20:1 (mol:mol) TxR-SE: $T_{349-biotin-IA}$] and the sample was incubated with shaking for 1 h at room temperature. To remove the unreacted TxR-SE, the sample was dialyzed against 5 L of Tris buffer, pH 8.2, overnight with one change of buffer. This was sufficient to remove the free TxR-SE to a level that contributed $\leq$5% of the fluorescence in the protein-containing sample.

The samples containing TxR-labeled $T_{349-biotin-IA}$ (TxR-$T_{349-biotin-IA}$) were preincubated with SA in the presence and absence of LUV at pH 4.5 and pH 8.2. To do this, a 7.5 μL aliquot from a 2 mg/mL solution of SA dissolved in water was added to a 25 μL aliquot of TxR-biotin-T and the mixture was incubated at room temperature for 20 min. Separately, 25 μL of a LUV preparation [10 mM 3:7 DOPG:DOPC (mol:mol) in the appropriate buffer] was mixed with 192.5 μL of acetate buffer, pH 4.5, or Tris buffer, pH 8.2. The LUV and TxR-$T_{349-biotin-IA}$/SA or TxR-$T_{349-biotin-IA}$ solutions were mixed. The samples were then diluted 2-fold to 0.5 mL with a solution containing 80% (w/v) sucrose dissolved in acetate or Tris buffer, as appropriate. The final concentrations of TxR-$T_{349-biotin-IA}$, SA, and lipid were 5 μg/mL, 30 μg/mL, and 0.5 mM, respectively. The samples were transferred to a 5 mL centrifuge tube and carefully overlaid with 3 mL of acetate or Tris buffer containing 25% (w/v) sucrose. Finally, 1 mL of acetate or Tris buffer without sucrose was carefully placed on top. The sample was then placed in a SW-60 rotor and centrifuged at 38000 rpm in a Beckman model L8-55 Ultracentrifuge for 3.5 h at 23 °C.

After centrifugation, the opaque lipid band was readily visible near the interface between the 0 and the 25% sucrose solutions. Fractionation of the sample was performed by cautiously collecting 0.45 mL aliquots from the very top of the gradient yielding 10 fractions in total. The TxR fluorescence was measured in each fraction as described above. The percentage of TxR fluorescence in each fraction was calculated with the following formula: $(F_{frac}/F_{total}) \times 100\%$, where F_{frac} is the fluorescence in an individual fraction and F_{total} is the sum of the fluorescence in all fractions. The average fluorescence from duplicate samples was calculated.

RESULTS

Strategy to Detect Biotinylated Residues Exposed to the trans Side of the Bilayer Using Vesicle-Entrapped BOD-SA. A spectroscopic biotin/SA assay was used to explore the topography of biotinylated T domain mutants inserted into lipid vesicles. Previous investigators had shown that the fluorescence of a BOD-labeled avidin increases upon addition to biotin and can be used to assay the exposure of biotinylated groups to avidin (*33*−*35*). We developed a variation of this assay for use with BOD-SA. Figure 3 illustrates how the BOD-SA assay would respond to different topographies (Figure 3, cases i−iii). When all of the biotin tags are attached to a residue face, the vesicle exterior (case i), an increase in BOD fluorescence intensity would be observed when BOD-SA is added externally to buffer-filled vesicles (Figure 3, top left) but not when BOD-SA is trapped inside the vesicle lumen (Figure 3, top center). The % of reactivity with external BOD-SA relative to total reactivity with external and trapped BOD-SA (= % external reactivity) would be equal to 100% (Figure 3 bottom, left). If the biotin tags face the interior of the vesicle (case ii), then an increase

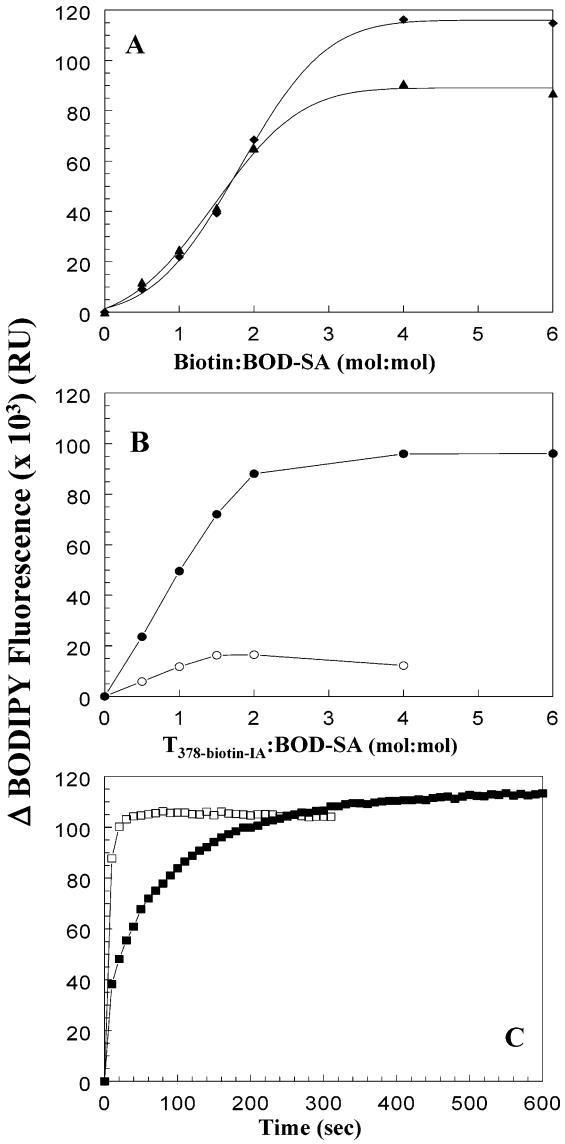

FIGURE 2: Fluorescence enhancement and kinetics of BOD-SA interaction with free biotin and biotinylated T domain. (A) Change in BOD fluorescence of 0.15 μg/mL BOD-SA upon addition of increasing amounts of free D-biotin at pH 8.0 (diamonds) or pH 4.5 (triangles). (B) Change in BOD fluorescence of 0.15 μg/mL BOD-SA upon addition of increasing amounts of $T_{378-biotin-IA}$ at pH 4.5 in the presence (filled circles) or absence (open circles) of 70% DOPC and 30% DOPG (mol:mol) SUV. The lipid concentration was 200 μM. (C) Change in BOD fluorescence as a function of time after the addition of 0.02 μM free D-biotin (open squares) or 0.02 μM (0.4 μg/mL) $T_{378-biotin-IA}$ (filled squares) to 0.15 μg/mL BOD-SA in the presence of SUV composed of 70% DOPC and 30% DOPG (mol:mol) at pH 4.5. The lipid concentration was 200 μM. The *Y*-axis in panels A−C indicates the increase in the raw BOD fluorescence upon the addition of free D-biotin or $T_{378-biotin-IA}$ in relative units (RU). The initial fluorescence values for 0.15 μg/mL BOD-SA were about 50×10^3 RU at pH 8.0 and 60×10^3 RU at pH 4.5 prior to addition of biotin. These and all subsequent experiments were carried out at room temperature. Panels A and C show representative examples of experiments performed multiple times.

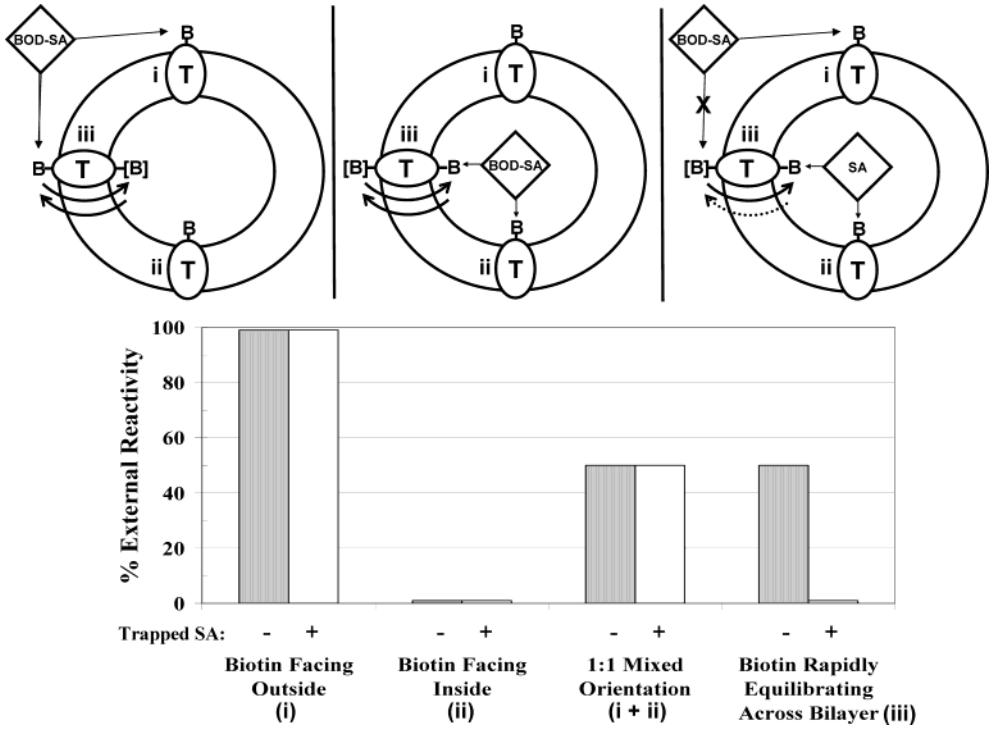

FIGURE 3: Schematic representation of BOD-SA assay used to detect residue exposure to different sides of the bilayer. Top: schematic representation of the interaction of BOD-SA (BOD-SA-labeled diamond) with the biotinylated T domain (oval) when BOD-SA is added externally to vesicles (left), entrapped inside vesicles (middle), or added externally to vesicles containing trapped unlabeled SA (SA-labeled diamond) (right). External BOD-SA is added to vesicles after T domain insertion. Biotinylated T domain molecules are illustrated in situations in which the biotin tag (B) is attached to a residue facing the outside of the vesicle (i), facing the inside of the vesicle (ii), or rapidly equilibrating (double arrows) back and forth across the bilayer (iii). In the case of biotin equilibration across the bilayer, the brackets denote the side on which biotin tags disappear due to reaction with either BOD-SA or SA. Bottom: theoretical values for % biotin reactivity with external BOD-SA relative to total reactivity with external and trapped BOD-SA under different conditions. Shaded bars: % external reactivity calculated for samples with external BOD-SA added to buffer-containing vesicles with the bound T domain (−). Open bars: % external reactivity calculated for samples with external BOD-SA added to vesicles with entrapped unlabeled SA and bound T domain (+).

in BOD fluorescence intensity would be observed with the vesicle-entrapped BOD-SA but not when BOD-SA was added externally. In that case, the % external reactivity would be 0% (Figure 3 bottom, second from left). Another possibility is that the T domain stably inserts in a mixed orientation with a certain fraction of the biotin tags facing the vesicle exterior and the remaining biotin tags facing the interior of the vesicle (a mixture of case i plus case ii). In this situation, the % external reactivity would reflect the fraction of biotin tags that are facing the vesicle exterior (Figure 3 bottom, second from right).

A final possibility is one in which a labeled residue is attached to a segment of the T domain that does not insert in a stable, fixed orientation but instead moves back and forth across the bilayer (case iii). In this case, the % external reactivity would have some intermediate value dependent on the rate of movement across the bilayer. If the rate of equilibration was rapid, the % external reactivity would be 50% (Figure 3, bottom right).

For the first three possibilities discussed above, preincubation of the biotinylated T domain with vesicle-entrapped unlabeled SA (Figure 3, top right) instead of buffer-filled vesicles (Figure 3, top left) would not affect the level of reactivity with subsequently added external BOD-SA (Figure 3, bottom, open bars). However, in the case of a rapid movement of a biotinylated segment of the protein back and forth across the bilayer, preincubation with vesicles containing trapped unlabeled SA would result in binding of the biotin to the unlabeled SA and thus suppressed reactivity with BOD-SA that was subsequently added externally (Figure 3, bottom right). The level to which the reactivity was suppressed by trapped SA would depend on the rate that the biotinylated group crosses the bilayer. Thus, by using vesicles containing trapped unlabeled SA, it is possible to distinguish intermediate values of % external reactivity arising from a stable mixed orientation from those arising from residues equilibrating across the bilayer.

Fluorescence Properties of BOD-SA upon Interaction with Biotin. Previous studies had shown that the fluorescence of BOD-avidin increases upon addition to biotin at neutral pH (*33*). Because we used BOD-SA in place of BOD-avidin and because membrane insertion of the T domain requires a low pH environment, the interaction of biotin with BOD-SA at low pH was studied to define conditions needed for the study of T domain topography. As shown in Figure 2A, titration of BOD-SA with increasing amounts of free D-biotin results in a similar increase in BOD fluorescence at both pH 4.5 and pH 8.5, indicating that the interaction is largely pH-independent in this range. We concluded that the BOD-SA can be substituted for BOD-avidin and used at a low pH. However, the initial BOD fluorescence of BOD-SA was higher at a low pH. This may mean that some BOD moves out of the biotin binding pocket on SA at a low pH even in the absence of biotin.

The titration of BOD-SA with the T domain having a biotin attached to a Cys introduced at residue 378 ($T_{378-biotin-IA}$) was also studied (Figure 2B). Residue 378 was labeled because it remains highly exposed to the external surface of

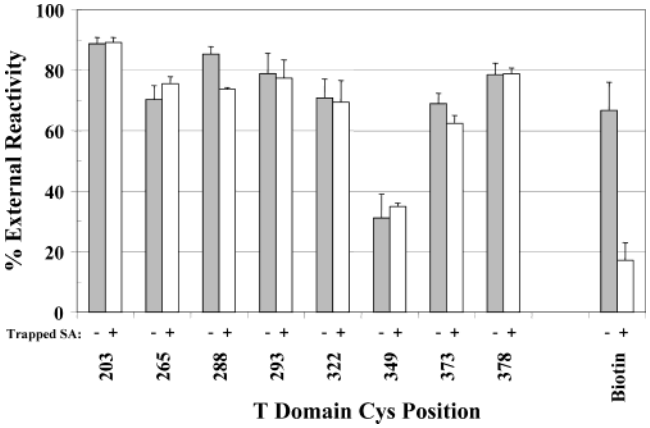

FIGURE 4: Percent external reactivity for biotinylated T domain mutants. The % external reactivity is shown for a series of biotinylated T domain Cys mutants using vesicles without (shaded bars, −) or with (open bars, +) 0.2 μg/mL entrapped unlabeled SA. Samples contained 2 μg/mL total T domain (0.2 μg/mL biotinylated T domain, 1.8 μg/mL unlabeled WT T), 0.2 μg/mL BOD-SA, and 0.19−0.22 mM lipid (70% DOPC and 30% DOPG LUV) in acetate buffer, pH 4.5. The *X*-axis numbers indicate the position of the biotinylated Cys in the T domain sequence. In the free biotin experiment, an amount of biotin equivalent to that in the protein-containing samples (0.01 μM) was used.

the bilayer when the T domain is inserted into SUV (*29*). The enhancement of BOD fluorescence in response to increasing amounts of $T_{378-biotin-IA}$ in the presence of SUV at a low pH was similar to that observed for free D-biotin. This indicates that attachment of the biotin molecule to the T domain does not hinder the interaction with BOD-SA. However, in the absence of SUV, there was very little interaction of $T_{378-biotin-IA}$ with BOD-SA at a low pH. This is most likely due to steric hindrance of SA binding to biotin arising from the low pH-induced T domain aggregation in solution (*4*).

The kinetics of the interaction of BOD-SA with $T_{378-biotin-IA}$ and free D-biotin was examined at a low pH in the presence of SUV (Figure 2C). The reaction rate was more rapid for biotin (complete within a minute) than for the biotinylated T domain (almost complete within 10 min). In the reaction of BOD-SA with other biotinylated T domain mutants, we studied displayed kinetics similar to those with $T_{378-biotin-IA}$ (data not shown). Because the reaction within the biotinylated T domain did increase a small amount after 10 min, an incubation time of 30 min was used in subsequent experiments.

Topography of Biotinylated T Domain as Determined by the BOD-SA Assay. Next, the BOD-SA topography assay was applied to a series of biotinylated T domain molecules. A set of 10 single Cys T domain mutants, mostly in the hydrophilic loop regions joining TH5−9, were labeled with biotin-IA. Their topographical location was assessed using LUV into which the externally added T domain was inserted at a low pH. Under these conditions, the T domain spontaneously forms the more deeply inserted "TM state" (*28*−*30*). Figure 4 shows the % external BOD-SA reactivity for these biotinylated proteins. In almost all cases, roughly 70−80% of the total BOD fluorescence increase was observed with externally added BOD-SA (Figure 4, shaded bars). This indicated that for most residues 70−80% of the SA reactive population was exposed to the external surface of the vesicle. (Because the T domain is added externally, the external surface is equivalent to the cis side of the bilayer.) The only exception to this pattern was residue 349 for which the % external reactivity was only 33%. This indicated that for most T domain molecules residue 349 reached the trans side of the bilayer. This was expected, because this residue is located in the very short loop region joining two transmembrane helices, TH8 and TH9 (see below).

These experiments were also carried out using T domains biotinylated on residues 311 or 356, both of which have previously been shown to be deeply buried in the bilayer when the T domain is in the TM state (*28*−*30*). Consistent with deep burial, the absolute BOD-SA fluorescence increase was 2−3 lower fold for residues 311 and 356 than for the other residues (data not shown). However, a residual fluorescence increase was observed. This was probably due to a subpopulation of proteins that did not insert in the TM state (see below). This reactive T domain subpopulation exhibited a % external reactivity of 70−75% (data not shown).

To determine whether the T domain residues were able to rapidly equilibrate across the bilayer, each biotinylated mutant T domain was preincubated with vesicles containing trapped unlabeled SA. Preincubation with vesicles containing trapped SA had little, if any, effect on the % external reactivity (Figure 4, open bars as compared to shaded bars). We concluded that the T domain stably inserted at a low pH, such that none of the residues examined were able to equilibrate across the membrane after insertion.

As a control to confirm that equilibration of biotin groups across the bilayer could be detected by this assay, we used free biotin. Free biotin can traverse the lipid bilayer (*34*, *35*). As shown in Figure 4, externally added biotin was able to react with trapped BOD-SA to some degree and preincubation of externally added free biotin with vesicles containing trapped unlabeled SA greatly reduced the % external reactivity with BOD-SA subsequently added externally relative to the % external reactivity when using buffer-containing vesicles (Figure 4, far right). These results confirm that the BOD-SA assay can detect the significant fraction of biotin that crosses the bilayer over the period of the assay.

Effect of Biotin Label on T Domain Topography. It was important to determine if biotinylation altered the T domain conformation or topography. We were initially concerned that a label with a long linker arm between the T domain and the biotin could lead to ambiguous results because the biotin might locate at a position in a membrane that is different from that of its attachment site. For this reason, biotin-IA, which has a shorter linker arm than most other available biotin probes, was chosen. Nevertheless, we decided to perform controls comparing biotin-IA to biotin-HPDP, a biotinylation reagent with a longer linker arm. The biotin-HPDP-labeled T domain had previously been used to detect the exposure of T domain residues to the trans side of planar lipid bilayers, and the biotin-HPDP label did not hinder T domain insertion under a variety of conditions (*27*). As shown in Figure 5, biotin-IA by itself translocates across bilayers much more slowly than biotin-HPDP. About 30% of the biotin-HPDP crossed the bilayer in 30 min. This suggested that biotin-HPDP would be less likely to prevent membrane penetration. However, this did not mean that biotin-IA would prevent membrane insertion. Attachment to a hydrophobic sequence should greatly enhance the ability

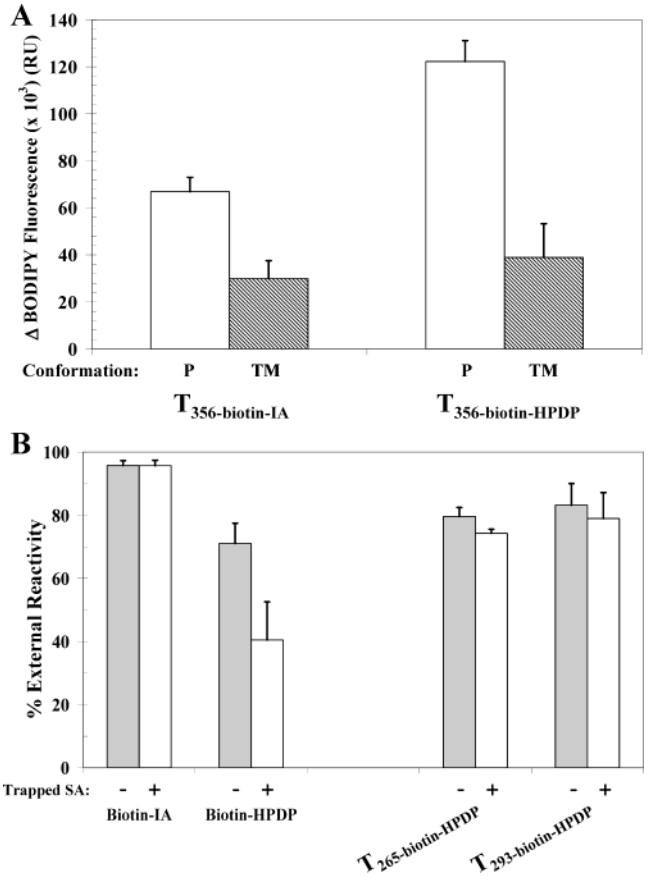

FIGURE 5: Effect of the type of biotin label used on reactivity with BOD-SA. T domain mutants with Cys at residues 265, 293, or 356 were labeled with biotin-IA or biotin-HPDP. (A) BOD fluorescence increase observed upon addition of externally added BOD-SA to SUV-bound $T_{356-biotin}$ inserted in the P state (vesicles composed of 70% DOPC and 30% DOPG) (open bars) or TM state (vesicles composed of 70% DMoPC and 30% DOPG) (striped bars) at pH 4.5. The lipid concentration was 200 μM. The *Y*-axis denotes BOD fluorescence in RU. (B) The % external reactivity is shown for free biotin labels (biotin-IA and biotin-HPDP) and LUV-inserted T domain mutants 265 and 293 labeled with biotin-HPDP, using vesicles without (shaded bars, −) or with (open bars, +) 0.2 μg/mL vesicle-entrapped unlabeled SA. The final concentration of the free biotin labels was 0.01 μM. All other conditions are as in Figure 4.

of a biotin label to penetrate the bilayer. This was confirmed by the observation that biotin-IA attached to residue 349 was able to cross bilayers (see above).

Nevertheless, we were concerned that biotin labeling would prevent proper membrane insertion under some conditions. Therefore, we examined whether biotin labeling by either of these biotinylation agents prevented proper insertion of the T domain. To do this, the interaction of biotinylated 356 with externally added BOD-SA was examined in the presence of SUV. Residue 356 was chosen because it is located in the hydrophobic portion of helix TH9 and becomes deeply buried in the bilayer when the T domain switches from the shallowly inserted P state to the more deeply inserting TM state (*29*). There was a significant decrease in reactivity of $T_{356-biotin}$ with externally added BOD-SA in the presence of DMoPC-containing SUV, in which the T domain forms the TM state (Figure 5A, striped bars), relative to that in DOPC-containing SUV, in which the T domain forms the P state (Figure 5A, open bars), for both biotin-IA and biotin-HPDP labeling agents. The decrease in reactivity (>50%) was similar to the previously observed decrease in anti-BOD antibodies binding to T domains labeled on residue 356 with hydrophobic BOD groups under similar conditions (*28*, *29*). This indicates an ability of both biotin-IA and biotin-HPDP labels attached to residue 356 to penetrate the bilayer.

Still, it is possible that biotin-IA labeling might give different topography results than biotin-HPDP labeling due to its lesser ability to penetrate the bilayer. In particular, we were concerned that the formation of a TM orientation by either TH5 or TH6/7 might be prevented due to biotin-IA labeling. To rule this out, the topographical locations of residues 265 and 293 were studied with biotin-HPDP. These residues are in the loops joining TH4 to TH5 and TH5 to TH6, respectively. If TH5 or TH6/7 formed a TM state, one or both of these residues would have to be located on the trans side of the bilayer. However, biotin-HPDP attached to the T domain containing Cys at residues 265 or 293 exhibited about 80% external reactivity, a value similar to that obtained with biotin-IA labeling (compare Figure 4 and Figure 5B), thus indicating a primarily cis location for these residues. It should be noted that in the open channel state a biotin-HPDP label attached to several residues N-terminal to TH5 (residues 235, 261, and 267) does move to the trans side of the bilayer, and thus, TH5 does form a TM helix in that state (*27*) (see Discussion). We concluded that it was very unlikely that the use of biotin-IA prevented TM insertion of helices 5−7.

Effect of SA Binding on Pore Formation. The ability of the T domain to form pores in lipid bilayers is believed to be a key feature of the mechanism of A chain translocation. To investigate the relationship between topography and pore formation, we assessed the effect of binding SA to the biotinylated T domain prior to membrane insertion upon subsequent pore formation by the T domain. The reasoning was that the binding of SA to a biotinylated residue should not greatly affect insertion or pore formation if attached to a residue that is exposed to the aqueous solution on the cis side of the bilayer in the membrane-inserted state. In contrast, because SA is a large and stably folded protein, it should not be able to move across the bilayer; thus, binding of SA to a residue that normally moves to the trans side of the bilayer should block proper insertion of that residue. In such a case, if the labeled residue were part of a sequence important for pore formation, SA binding would block pore formation.

To assay for pore formation, we measured the influx of CB dye molecules into the vesicles. This was detected by fluorescence quenching of externally added CB by vesicle-entrapped anti-CB antibodies (*11*). [Antibodies are too large to escape vesicles through the T domain-induced pores (*11*, *12*, *14*, *36*, *37*).] One advantage of measuring influx was that the CB could be added after the T domain was preincubated with the vesicles. This eliminated the possibility of CB influx due to transient lesions in vesicle integrity that might exist only at the moment of T domain insertion.

We first characterized the dependence of pore formation upon T domain concentration. Figure 6A shows that the % quenching of CB fluorescence increased linearly with an increasing T domain concentration. This means that the concentration of pore-forming T domain molecules in a sample should be linearly reflected in the % quenching of

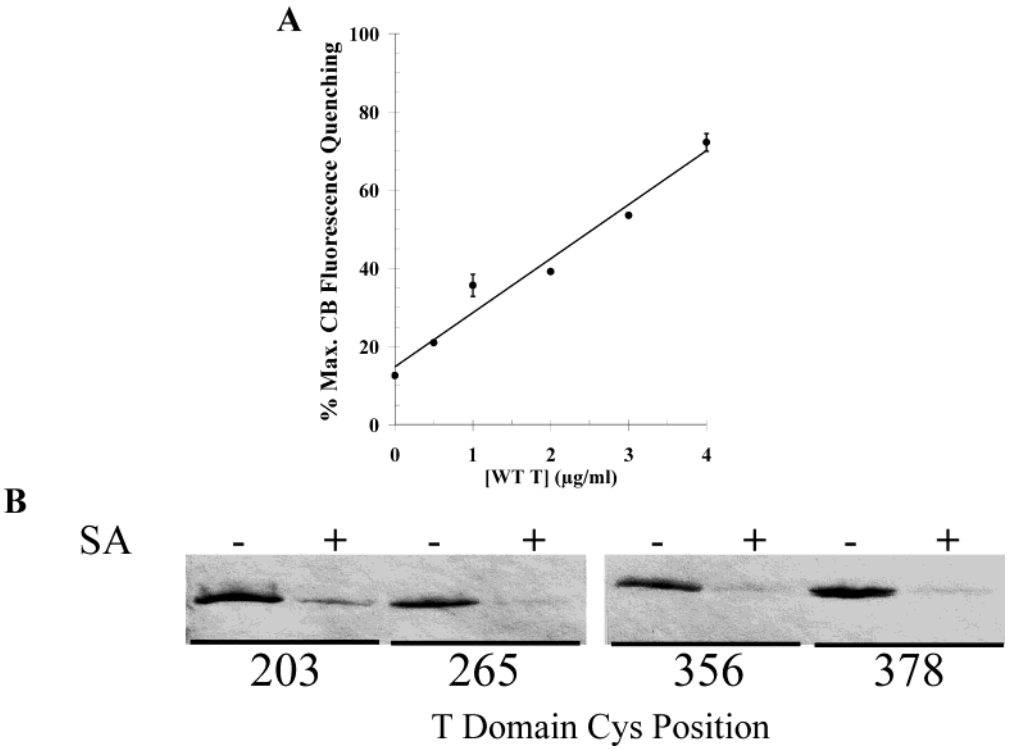

FIGURE 6: Pore formation by the WT T domain and analysis of SA binding to biotinylated T domain mutants. (A) The effect of T domain concentration on CB influx into vesicles containing trapped anti-CB antibodies. Various amounts of the WT T domain were added to LUV composed of 70% DOPC and 30% DOPG and containing ~0.05 μM trapped anti-CB at pH 4.5. The lipid concentration was 200 μM. After 15 min, an aliquot of CB was added to a final concentration of ~2 nM. The fluorescence was measured after a 1 h of incubation. The % maximum CB fluorescence quenching is % quenching/% quenching in the presence of excess octyl glucoside. (B) SDS−PAGE of 0.1 mg/mL biotinylated T domain mutants preincubated with (+ lanes) and without (− lanes) 0.6 mg/mL SA in Tris buffer, pH 8.2. Numbers refer to the residue that is labeled. The disappearance of the free T domain band reflects the formation of higher molecular weight T domain-SA complexes. (Bands representing T domain-SA complexes were detected but were not analyzed because they corresponded to a mixture with various stoichiometries and overlapped the diffuse free SA band.) All other biotinylated T domain mutants tested yielded similar results to those shown.

CB fluorescence. [Because the T domain has been known to cause vesicle fusion (*38*), we were concerned that a fraction of the CB quenching that we observed was due to CB leaking into vesicles during vesicle fusion rather than via T domain-induced pores. This possibility was ruled out using a fluorescence resonance energy transfer-based lipid mixing assay (*39*). In control experiments, we found negligible fusion during the CB influx assay period, which starts after preincubation of the T domain with vesicles (data not shown).]

Next, we tested a series of biotinylated T domain mutants for their ability to form pores (Figure 7). Addition of the biotinylated T domain mutants to vesicles resulted in a level of CB fluorescence quenching similar to that observed with the unbiotinyated WT T domain (Figure 7, open bars). This indicated that biotin labeling did not significantly interfere with the ability of the T domain to form pores.

The effect of prebound SA upon pore formation was then examined. Unless otherwise noted, we confirmed that almost all of the biotinylated T domain mutants had bound to SA prior to addition to vesicles (some examples are shown in Figure 6B). Complexes of SA with mutants biotinylated on residues predominantly exposed to aqueous solution on the cis bilayer surface (residues 203, 265, 288, 293, and 378) showed that the bound SA had little or no effect on the amount of CB fluorescence quenching (Figure 7, shaded bars). This is consistent with the expectation that binding of SA to such residues should not interfere with normal membrane insertion. An alternative interpretation is that these residues may reside in parts of the protein that are not critical for pore formation.

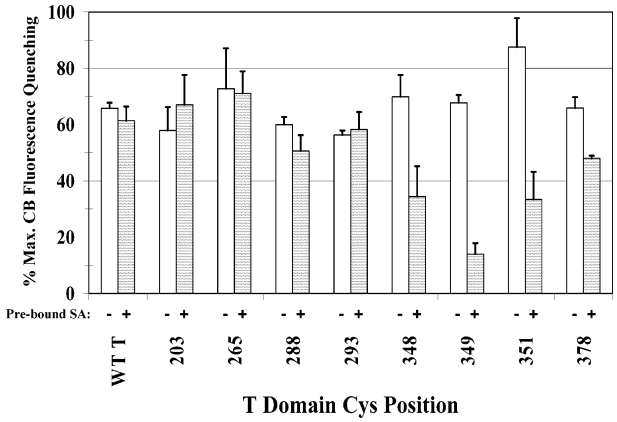

FIGURE 7: Effect of SA-T domain complex formation upon T domain-induced pore formation. The effect of biotinylated T domain mutants upon CB influx into LUV was measured as described in Figure 6A. Samples contained 4 μg/mL biotinylated T domain (open bars) or 4 μg/mL biotinylated T domain complexed with 24 μg/mL SA prior to addition of LUV (striped bars). WT = unbiotinylated WT T domain.

In contrast to the binding of SA to predominantly cis side-locating residues, binding of SA drastically reduced the amount of CB quenching observed when biotin was attached to the predominantly trans side-locating residue 349. A reduction in CB quenching was also observed when SA was

bound to a biotin attached to residues 348 and 351, although to a somewhat lesser extent.

One explanation for the ability of SA to inhibit pore formation of T domain molecules biotinylated on residues 348, 349, and 351 is that attaching a SA molecule to the short loop region between TH8 and TH9 (residues 347−355) severely disrupts pore formation by blocking the movement of this loop region to the trans surface. This is consistent with topography data indicating that this loop is the only portion of the T domain that reaches the trans side of the bilayer. Incomplete blockage of pore formation in complexes of SA with $T_{349-biotin-IA}$ could be due to the fact that the minor subpopulation of T domain molecules with an inverted orientation can still insert properly. The lesser blockage of quenching observed with complexes of SA and $T_{348-biotin-IA}$ and $T_{351-biotin-IA}$ may partly be due to fact that these biotinylated residues exhibited slightly less complete binding to SA in solution (data not shown).

An alternate possibility is that residues 348, 349, and 351 are located at the opening of the pore and bound SA partially occludes pore formation sterically. This is consistent with the observation that in the open channel state the pore is formed by the TH8/TH9 transmembrane hairpin (*19*). However, this explanation seems unlikely because it requires that SA translocates such that TH8 and TH9 can form a normal TM hairpin.

On the other hand, it is quite possible that partial occlusion of the pore opening is responsible for the (small) inhibition of pore formation upon SA binding to a biotin attached to the TH9-bordering residue 378. Residue 378 remains on the cis surface of the bilayer, and so, this mechanism of inhibition would not require translocation of SA.

An additional trivial explanation for the loss of pore formation would be that SA bound to residues such as 349 prevented the T domain from binding to lipid vesicles. To test this, we fluorescently labeled $T_{349-biotin-IA}$ with amine-reactive TxR and analyzed its ability to bind to LUV after preincubation with SA on a sucrose density gradient.

When a complex of TxR-labeled $T_{349-biotin-IA}$ and SA was added to LUV at low pH, ~90% of the TxR fluorescence was found in the lipid-containing fractions near the top of the gradient, whereas in the absence of lipid the protein complex remained at the bottom of the gradient (data not shown). In addition, in the presence of LUV at a high pH, a condition in which the T domain remains folded and does not strongly interact with lipid (*40*), ~90% of the TxR fluorescence remained at the bottom of the gradient (data not shown). These data indicate that SA binding to residue 349 does not prevent the T domain from binding to lipid.

Finally, we tested the effect of SA binding upon pore formation using biotinylated residues within hydrophobic sequences (residues 311 and 356). SA binding to neither residue 311 nor 356 affected the amount of CB quenching observed (data not shown). This was true even when residue 356 was labeled with the more membrane permeable biotin-HPDP. Possible explanations for these observations are considered in the Discussion.

DISCUSSION

Use of BOD-SA to Probe Topography, Orientation, and Equilibration across Bilayers. Defining the topography of the membrane-inserted T domain is a key step necessary for understanding the mechanism by which it facilitates the translocation of the toxin's catalytic domain across a lipid bilayer. Unfortunately, protein toxins such as DT are among the most challenging targets for topographical analysis. Unlike ordinary membrane proteins, they tend to have membrane-penetrating segments with hydrophobicity values that are sufficiently low as to be ambiguous indicators of transmembrane orientation. In addition, they can exist in a number of conformations and orientations depending on experimental conditions (*28*−*30*, *41*, *42*). Such conformational flexibility may be inherent to their ability to carry out protein translocation but multiplies the difficulty of topographical analysis. Finally, they often insert only under conditions (such as low pH) that rule out and/or greatly complicate a variety of conventional methods for the analysis of topography.

Our previous studies allowed us to limit the possible arrangements of TH5−9 in the membrane-inserted state (*30*). However, a more definitive topography required methods to detect if specific residues reach the trans side of the membrane and if they did so in a stable fashion. To accomplish this, we developed a biotin/SA-based approach. We previously used SA binding to crudely assay the topography of intact DT-containing biotinylated Lys (*8*). The effect upon channel formation of SA binding to individual biotinylated Cys residues has previously been studied in much more detail for the membrane-inserted T domain and for membrane-inserted colicin Ia, to identify which residues reside on the cis and trans sides of the bilayer when these proteins are in the open channel conformation (*27*, *41*, *43*, *44*).

SA binding to membrane-inserted proteins can also be assessed spectroscopically. Biotin binding to BOD-labeled avidin can be detected because it displaces BOD from the biotin binding pocket, in which its fluorescence is thought to be quenched by Trp residues (*33*). The fluorescence enhancement of a BOD-avidin conjugate upon its binding to biotin that was attached to the GALA peptide has been used to determine GALA orientation in lipid bilayers (*34*, *35*). Here, we have further refined this approach by using BOD-SA. SA is nonglycosylated and has a neutral isoelectric point, factors that should reduce interference from electrostatic interactions of avidin with lipid. More importantly, we introduced protocols for detecting cases in which residues equilibrate back and forth across the bilayer. Using this approach, we could fully evaluate the exposure of individual residues to the cis and trans sides of the bilayer.

Topography of the Membrane-Inserted T Domain: Formation of a Stable, Nonclassical Topography by Helices 5−*7.* Combining the results of the BOD-SA topography analysis with our previous results (*30*) allows us to propose a topography for the membrane-inserted T domain at a low pH (Figure 8, top). The results obtained from the BOD-SA assay showed that of the residues studied only 349, located in the short loop region joining TH8 and TH9, reaches the trans side of the membrane. [The locations of two other residues in this loop region, 348 and 351, were also tested. However, they displayed virtually no reaction with either externally added or vesicle-entrapped BOD-SA, most likely due to the fact that they are not close enough to the trans bilayer surface to react with the BOD-SA (data not shown).

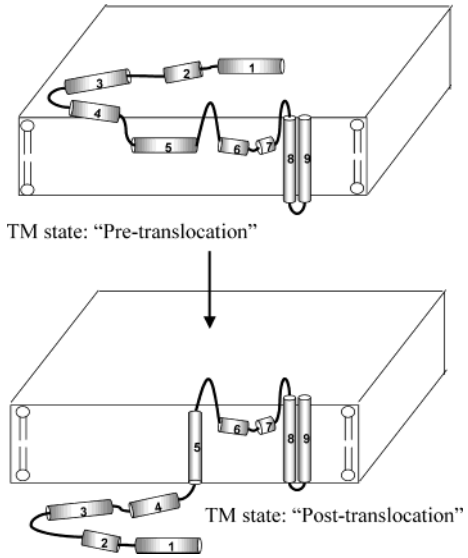

FIGURE 8: Models for the topography of the T domain at different stages of translocation. T domain helices are numbered as defined in Choe et al. (*1*). Top: schematic representation of the topography of the deeply membrane-inserted T domain at low pH (TM state) derived from the data obtained in this and previous studies (*29*, *30*). Bottom: model for the T domain in the open channel state as proposed by Senzel et al. (*27*) in the presence of a pH gradient (cis, pH 5; trans, pH 7). Because the N-terminal of the T domain would be attached to the A chain, the low pH topography (top) may represent an early stage in the translocation process (A chain on cis side of bilayer) while the open channel topography (bottom)-may represent a later stage in which translocation is complete (A chain on trans side of bilayer). Note that the membrane-inserted hydrophobic helices may be more tightly packed with each other than shown schematically.

In some preparations we also saw reactivity of BOD-SA with T domain labeled on residue 349 that was too low for determining topography (data not shown). We believe this reflects the fact that residue 349 just barely reaches to the trans side of the bilayer.]

In contrast to the trans side localization of residue 349, residues located at the N-terminal of TH8 (322) and the C-terminal of TH9 (373, 378) remained on the cis side of the bilayer. These findings show definitively that TH8 and TH9 form a transmembrane hairpin. TH5 and the combination of TH6 and TH7 are a second set of hydrophobic segments that could potentially form a transmembrane hairpin. Our previous results showed that both TH5 and TH6/7 insert deeply into bilayers at low pH (*30*). However, formation of a transmembrane hairpin by these helices is ruled out by the observation that residues at both the N and C termini of TH5 and the N and C termini of the TH6/7 segment (265, 288, 293, and 322) remain on the cis side of the bilayer. These data also demonstrate that neither TH5 nor TH6/7 form transmembrane segments by themselves. Thus, we propose that TH5−7 form a novel nonclassical membrane protein structure in which they form a stable deeply inserted non-TM state.

Our model for the TH5−7 region (i.e., deeply inserted but not TM) is consistent with studies in cells showing that only the N-terminal portion of the T domain up to residue 264 was digested by an externally added protease. This implied that TH5−9 are buried in the bilayer (*22*, *24*). Deep insertion of TH5 is also consistent with the observations that the natural Trp in the center of helix 5 inserted into lipid bilayers (*25*) and that TH5 is labeled by hydrophobic photolabeling agents (*26*).

Our conclusion that TH8 and TH9 are transmembraneous while TH5−7 are not transmembraneous is consistent with additional protease studies in lipid vesicles (*16*). Those studies showed that TH8 and TH9 are protected from proteases even under conditions in which even TH5−7 are completely digested, suggesting a deeper insertion of TH8 and TH9 than of TH5−7. This is also consistent with our previous studies, which indicated that even in the deeply inserted state residues in the hydrophobic segments of TH5−7 were able to bind to external antibodies to a somewhat greater extent than residues in TH8 and TH9 (*30*).

A final piece of topographical information from the present study comes from the location of the N terminus of the T domain (residue 203). This was found to be located on the cis side of the bilayer, which suggests that in contrast to the open channel state (*27*), the TH1−4 region does not translocate across the membrane at low pH.

Contrast between Topography in TM and Open Channel States: Does the Low pH Topography Reflect an Early Step in the Translocation Process? As noted above, the topography of the T domain that we observed in the low pH TM state differs from that in the previously characterized open channel state, where TH1−4 are located on the trans side of the bilayer and TH5 spans the membrane (Figure 8, bottom) (*27*). Because the N-terminal of the T domain is on the cis side of the bilayer in the low pH TM state, we propose that it reflects an early stage in the translocation process, while the open channel state represents a later stage in which translocation of the N-terminal has already taken place.

The difference between these states may reflect the difference in experimental conditions. Our studies were conducted at a symmetric low pH in the absence of a membrane potential. In contrast, the open channel state is most efficiently formed when both a pH gradient (pH 5 cis, pH 7 trans) and a cis negative membrane potential exist across the bilayer, conditions known to be favorable to translocation (*9*, *45*−*49*). The conformational differences between these states may also be responsible for differences between their channel/pore properties (see below).

Relationship between Proper Insertion of T Domain Helices and Pore Formation. To examine the relationship between topography and pore formation, we examined the effect of prebinding SA to the biotinylated T domain upon the ability of the T domain to form pores in vesicles. Attaching a very large, tightly folded protein like SA to a residue on the T domain should disrupt pores if it blocks the proper transmembrane insertion of a portion of the T domain essential for pore formation.

On the basis of the BOD-SA results, one would predict that preventing the proper insertion of TH8 and TH9 alone should block pore formation because these are the only two helices that adopt a transmembrane conformation. This was observed. SA binding to residues 348, 349, and 351 inhibited pore formation. In contrast, the binding of SA to residues 203 and 265 (in TH1 and TH4, respectively) had no effect on pore formation. This implies that the translocation of this portion of the T domain is not necessary for the formation of pores at low pH. However, Senzel et al. observed that prebinding SA to residue 235 (located in the loop joining TH2 and TH3) prevented the formation of open channels

(*27*). This was one piece of data indicating that the translocation of the TH1−4 region did occur in the open channel state. The difference between these results further supports our conclusion that the open channel and low pH states are conformationally different.

We also found that SA bound to residue 311 in the middle of the hydrophobic TH6/7 stretch had no effect on CB uptake suggesting that TH6/7 does not play an important role in pore formation. However, these experiments are not definitive. Other experiments showed that SA binding to residue 356 did not inhibit pore formation. This is surprising because 356 is in the core of TH9, and interruption of its insertion should block pore formation if, as shown for the open channel state, the pore was formed solely by TH8 and TH9 (*19*). One possibility to explain this result is that the segments of the protein participating in pore formation depend on experimental conditions. If insertion of TH9 is partially blocked, TH8 and TH6/7 might form an alternate pore-forming structure. Alternatively, there might be a pore formed by other portions of the T domain molecule. These possibilities are consistent with experiments using T domains carrying mutations that prevent proper TH9 insertion (Zhao, G., and London, E. Unpublished observations). In fact, a study on the structurally related channel-forming domain of colicin Ia indicated that more than one set of inserted helices in the open channel state could exhibit pore formation (*41*).

It is noteworthy that the approach that we developed for examining pore formation (*11*) uses an externally added dye instead of one entrapped in the vesicles. Because it only detects pores that are present at the time at which the dye is added to the vesicles, it avoids interference from any transient leakiness that may develop at the time of toxin insertion into the lipid bilayer. This artifact has complicated many previous studies of pore formation.

T Domain Inserts in a Mixed Orientation. Interestingly, for most residues examined, some reactivity was observed with both externally added and vesicle-entrapped BOD-SA. This was shown not to involve equilibration of T domain sequences across the bilayer. Instead, the data imply that the T domain inserts with a mixture of orientations such that the N-terminal outside orientation comprises about 70−80% of all molecules. A mixture of orientations was also previously observed with whole toxin (*50*). While the biological significance of mixed orientations, if any, is unclear, we cannot rule out that the toxin inserts in a mixture of orientations in vivo. Oligomerization between toxin molecules oriented in different directions also cannot be ruled out. On the other hand, the mixture of orientations may simply be an artifact of the insertion protocol. Further experiments will be necessary to distinguish between these possibilities.

REFERENCES

1. Choe, S., Bennett, M. J., Fujii, G., Curmi, P. M., Kantardjieff, K. A., Collier, R. J., and Eisenberg, D. (1992) The crystal structure of diphtheria toxin, *Nature 357*, 216−222.
2. Bennett, M. J., Choe, S., and Eisenberg, D. (1994) Refined structure of dimeric diphtheria toxin at 2.0 Å resolution, *Protein Sci. 3*, 1444−1663.
3. Bennett, M. J., and Eisenberg, D. (1994) Refined structure of monomeric diphtheria toxin at 2.3 Å resolution, *Protein Sci. 3*, 1464−1475.
4. Bell, C. E., and Eisenberg, D. (1997) Crystal structure of nucleotide-free diphtheria toxin, *Biochemistry 36*, 481−488.
5. Pappenheimer, A. M., Jr. (1977) Diphtheria toxin, *Annu. Rev. Biochem. 46*, 69−94.
6. Umata, T., and Mekada, E. (1998) Diphtheria toxin translocation across endosome membranes. A novel cell permeabilization assay reveals new diphtheria toxin fragments in endocytic vesicles, *J. Biol. Chem. 273*, 8351−8359.
7. Oh, K. J., Senzel, L., Collier, R. J., and Finkelstein, A. (1999) Translocation of the catalytic domain of diphtheria toxin across planar phospholipid bilayers by its own T domain, *Proc. Natl. Acad. Sci. U.S.A. 96*, 8467−8470.
8. Jiang, J. X., Chung, L. A., and London, E. (1991) Self-translocation of diphtheria toxin across model membranes, *J. Biol. Chem. 266*, 24003−24010.
9. Beaumelle, B., Bensammar, L., and Bienvenue, A. (1992) Selective translocation of the A chain of diphtheria toxin across the membrane of purified endosomes, *J. Biol. Chem. 267*, 11525−11531.
10. Ratts, R., Zeng, H., Berg, E. A., Blue, C., McComb, M. E., Costello, C. E., vanderSpek, J. C., and Murphy, J. R. (2003) The cytosolic entry of diphtheria toxin catalytic domain requires a host cell cytosolic translocation factor complex, *J. Cell Biol. 160*, 1139−1150.
11. Sharpe, J. C., and London, E. (1999) Diphtheria toxin forms pores of different sizes depending on its concentration in membranes: probable relationship to oligomerization, *J. Membr. Biol. 171*, 209−221.
12. Kagan, B. L., Finkelstein, A., and Colombini, M. (1981) Diphtheria toxin fragment forms large pores in phospholipid bilayer membranes, *Proc. Natl. Acad. Sci. U.S.A. 78*, 4950−4954.
13. Papini, E., Sandona, D., Rappuoli, R., and Montecucco, C. (1988) On the membrane translocation of diphtheria toxin: at low pH the toxin induces ion channels on cells, *EMBO J. 7*, 3353−3359.
14. Sandvig, K., and Olsnes, S. (1988) Diphtheria toxin-induced channels in vero cells selective for monovalent cations, *J. Biol. Chem. 263*, 12352−12359.
15. Mindell, J. A., Zhan, H., Huynh, P. D., Collier, R. J., and Finkelstein, A. (1994) Reaction of diphtheria toxin channels with sulfhydryl-specific reagents: observation of chemical reactions at the single molecule level, *Proc. Natl. Acad. Sci. U.S.A. 91*, 5272−5276.
16. Quertenmont, P., Wattiez, R., Falmagne, P., Ruysschaert, J. M., and Cabiaux, V. (1996) Topology of diphtheria toxin in lipid vesicle membranes: a proteolysis study, *Mol. Microbiol. 21*, 1283−1296.
17. Zhan, H., Oh, K. J., Shin, Y. K., Hubbell, W. L., and Collier, R. J. (1995) Interaction of the isolated transmembrane domain of diphtheria toxin with membranes, *Biochemistry 34*, 4856−4863.
18. Zhan, H., Choe, S., Huynh, P. D., Finkelstein, A., Eisenberg, D., and Collier, R. J. (1994) Dynamic transitions of the transmembrane domain of diphtheria toxin: disulfide trapping and fluorescence proximity studies, *Biochemistry 33*, 11254−11263.
19. Silverman, J. A., Mindell, J. A., Zhan, H., Finkelstein, A., and Collier, R. J. (1994) Structure−function relationships in diphtheria toxin channels: I. Determining a minimal channel-forming domain, *J. Membr. Biol. 137*, 17−28.
20. Oh, K. J., Zhan, H., Cui, C., Altenbach, C., Hubbell, W. L., and Collier, R. J. (1999) Conformation of the diphtheria toxin T domain in membranes: a site-directed spin-labeling study of the TH8 helix and TL5 loop, *Biochemistry 38*, 10336−10343.
21. Oh, K. J., Zhan, H., Cui, C., Hideg, K., Collier, R. J., and Hubbell, W. L. (1996) Organization of diphtheria toxin T domain in bilayers: a site-directed spin labeling study, *Science 273*, 810−812.
22. Moskaug, J. O., Stenmark, H., and Olsnes, S. (1991) Insertion of diphtheria toxin B-fragment into the plasma membrane at low pH. Characterization and topology of inserted regions, *J. Biol. Chem. 266*, 2652−2659.
23. Madshus, I. H. (1994) The N-terminal alpha-helix of fragment B of diphtheria toxin promotes translocation of fragment A into the cytoplasm of eukaryotic cells, *J. Biol. Chem. 269*, 17723−17729.
24. Cabiaux, V., Quertenmont, P., Conrath, K., Brasseur, R., Capiau, C., and Ruysschaert, J. M. (1994) Topology of diphtheria toxin B fragment inserted in lipid vesicles, *Mol. Microbiol. 11*, 43−50.
25. Malenbaum, S. E., Collier, R. J., and London, E. (1998) Membrane topography of the T domain of diphtheria toxin probed with single tryptophan mutants, *Biochemistry 37*, 17915−17922.
26. D'Silva, P. R., and Lala, A. K. (2000) Organization of diphtheria toxin in membranes—A hydrophobic photolabeling study, *J. Biol. Chem. 275*, 11771−11777.

27. Senzel, L., Gordon, M., Blaustein, R. O., Oh, K. J., Collier, R. J., and Finkelstein, A. (2000) Topography of diphtheria Toxin's T domain in the open channel state, *J. Gen. Physiol. 115*, 421−434.
28. Wang, Y., Malenbaum, S. E., Kachel, K., Zhan, H., Collier, R. J., and London, E. (1997) Identification of shallow and deep membrane-penetrating forms of diphtheria toxin T domain that are regulated by protein concentration and bilayer width, *J. Biol. Chem. 272*, 25091−25098.
29. Kachel, K., Ren, J., Collier, R. J., and London, E. (1998) Identifying transmembrane states and defining the membrane insertion boundaries of hydrophobic helices in membrane-inserted diphtheria toxin T domain, *J. Biol. Chem. 273*, 22950−22956.
30. Rosconi, M. P., and London, E. (2002) Topography of helices 5−7 in membrane-inserted diphtheria toxin T domain: identification and insertion boundaries of two hydrophobic sequences that do not form a stable transmembrane hairpin, *J. Biol. Chem. 277*, 16517−16527.
31. Ren, J., Kachel, K., Kim, H., Malenbaum, S. E., Collier, R. J., and London, E. (1999) Interaction of diphtheria toxin T domain with molten globule-like proteins and its implications for translocation, *Science 284*, 955−957.
32. Senzel, L., Huynh, P. D., Jakes, K. S., Collier, R. J., and Finkelstein, A. (1998) The diphtheria toxin channel-forming T domain translocates its own NH2-terminal region across planar bilayers, *J. Gen. Physiol. 112*, 317−324.
33. Emans, N., Biwersi, J., and Verkman, A. S. (1995) Imaging of endosome fusion in BHK fibroblasts based on a novel fluorimetric avidin−biotin binding assay, *Biophys J. 69*, 716−728.
34. Nicol, F., Nir, S., and Szoka, F. C., Jr. (1999) Orientation of the pore-forming peptide GALA in POPC vesicles determined by a BODIPY-avidin/biotin binding assay, *Biophys. J. 76*, 2121−2141.
35. Nir, S., Nicol, F., and Szoka, F. C., Jr. (1999) Surface aggregation and membrane penetration by peptides: relation to pore formation and fusion, *Mol. Membr. Biol. 16*, 95−101.
36. Donovan, J. J., Simon, M. I., Draper, R. K., and Montal, M. (1981) Diphtheria toxin forms transmembrane channels in planar lipid bilayers, *Proc. Natl. Acad. Sci. U.S.A. 78*, 172−176.
37. Alder, G. M., Bashford, C. L., and Pasternak, C. A. (1990) Action of diphtheria-toxin does not depend on the induction of large, stable pores across biological-membranes, *J. Membr. Biol. 113*, 67−74.
38. Papini, E., Colonna, R., Cusinato, F., Montecucco, C., Tomasi, M., and Rappuoli, R. (1987) Lipid interaction of diphtheria toxin and mutants with altered fragment B. 1. Liposome aggregation and fusion, *Eur. J. Biochem. 169*, 629−635.
39. Tortorella, D., Ulbrandt, N. D., and London, E. (1993) Simple centrifugation method for efficient pelleting of both small and large unilamellar vesicles that allows convenient measurement of protein binding, *Biochemistry 32*, 9181−9188.
40. Chenal, A., Nizard, P., Forge, V., Pugniere, M., Roy, M. O., Mani, J. C., Guillain, F., and Gillet, D. (2002) Does fusion of domains from unrelated proteins affect their folding pathways and the structural changes involved in their function? A case study with the diphtheria toxin T domain, *Protein Eng. 15*, 383−391.
41. Qiu, X. Q., Jakes, K. S., Kienker, P. K., Finkelstein, A., and Slatin, S. L. (1996) Major transmembrane movement associated with colicin Ia channel gating, *J. Gen. Physiol. 107*, 313−328.
42. Jiang, J. X., Abrams, F. S., and London, E. (1991) Folding changes in membrane-inserted diphtheria toxin that may play important roles in its translocation, *Biochemistry 30*, 3857−3864.
43. Qiu, X. Q., Jakes, K. S., Finkelstein, A., and Slatin, S. L. (1994) Site-specific biotinylation of colicin Ia. A probe for protein conformation in the membrane, *J. Biol. Chem. 269*, 7483−7488.
44. Slatin, S. L., Qiu, X. Q., Jakes, K. S., and Finkelstein, A. (1994) Identification of a translocated protein segment in a voltage-dependent channel. *Nature 371*, 158−161.
45. Hudson, T. H., Scharff, J., Kimak, M. A. G., and Neville, D. M. (1988) Energy-requirements for diphtheria-toxin translocation are coupled to the maintenance of a plasma-membrane potential and a proton gradient, *J. Biol. Chem. 263*, 4773−4781.
46. Sandvig, K., and Olsnes, S. (1980) Diphtheria-toxin entry into cells is facilitated by low pH, *J. Cell Biol. 87*, 828−832.
47. Sandvig, K., and Olsnes, S. (1986) Interactions between diphtheria toxin entry and anion transport in Vero cells. IV. Evidence that entry of diphtheria toxin is dependent on efficient anion transport, *J. Biol Chem. 261*, 1570−1575.
48. Sandvig, K., and Olsnes, S. (1981) Rapid entry of nicked diphtheria toxin into cells at low pH. Characterization of the entry process and effects of low pH on the toxin molecule, *J. Biol. Chem. 256*, 9068−9076.
49. Marnell, M. H., Shia, S. P., Stookey, M., and Draper, R. K. (1984) Evidence for penetration of diphtheria toxin to the cytosol through a prelysosomal membrane, *Infect. Immun. 44*, 145−150.
50. Tortorella, D., Sesardic, D., Dawes, C. S., and London, E. (1995) Immunochemical analysis shows all three domains of diphtheria toxin penetrate across model membranes, *J. Biol. Chem. 270*, 27446−27452.

BI049354J